International Journal of Biological Macromolecules 164 (2020) 2881–2894

Contents lists available at ScienceDirect

International Journal of Biological Macromolecules

journal homepage: http://www.elsevier.com/locate/ijbiomac

Dual cancer targeting using estrogen functionalized chitosan nanoparticles loaded with doxorubicin-estrone conjugate: A quality by design approach

Balak Das Kurmi [a], Rishi Paliwal [b], Shivani Rai Paliwal [a,*]

[a] Pharmaceutics Research Laboratory, SLT Institute of Pharmaceutical Sciences, Guru Ghasidas Vishwavidyalaya, Bilaspur 495009, CG, India
[b] Nanomedicine and Bioengineering Research Laboratory, Department of Pharmacy, Indira Gandhi National Tribal University, Amarkantak 4848487, MP, India

ARTICLE INFO

Article history:
Received 26 March 2020
Received in revised form 14 August 2020
Accepted 21 August 2020
Available online 24 August 2020

Keywords:
Nanoparticles
Chitosan
Doxorubicin
Estrogen receptor
Dual targeting
Quality by design
Box–Behnken design

ABSTRACT

In this study, estrone was used as targeting functionality in chitosan nanoparticles (DoxEs-CSEsNPs) carrying doxorubicin-estrone conjugate for dual targeted intracellular delivery to breast cancer cells. Estrone was conjugated with Dox and CS and characterized by FTIR and FT-NMR spectroscopy. Dox/DoxEs containing CSEsNPs were prepared with ionic gelation method and for the effect of formulation variables a 3-factor, 3-level Box-Behnken design (BBD) was explored, which predict the responses like particle size (Y_1) and percent entrapment efficiency (%EE) (Y_2) when CSEs: TPP ratio (X_1), sonication time (X_2) and stirring speed (X_3) were selected as independent variables. The Dox-CSEsNPs and DoxEs-CSEsNPs were characterized for size, shape, PDI, surface charge and thermal analysis. The drug entrapment efficiency was 66.33 ± 2.82% and 62.25 ± 2.63% for Dox-CSEsNPs and DoxEs-CSEsNPs formulation respectively. The in vitro release, haemolytic toxicity, and fluorescent microscopy studies were also assessed. Anticancer activity on the MCF-7 cell line indicated the higher potency of DoxEs-CSEsNPs as compared to Dox-CSEsNPs, DoxEs, and Dox solution. The findings are decisive for selective targeting of antineoplastic agents to the ERs, which indicate that the DoxEs loaded CSEsNPs were able to significantly improve the efficacy of Dox.

1. Introduction

Breast cancer is a frequently occurring cancer among women and presents significant challenges for its treatment. Conventional breast cancer therapy has several obstacles such as non-specific biodistribution of the drug, low intracellular drug concentration, and occurrence of multidrug resistance [1,2]. Tumor cell targeting could be an option for breast cancer treatment that would evade the limitations of conventional chemotherapy. A number of molecular targets have been identified on the basis of pathophysiology of cancer cells that can be utilized for targeted breast carcinoma therapy [3,4].

Breast cancer is classified on the basis of expression of hormone receptors or target protein such as hormone receptor positive cancer (i.e. estrogen receptor or progesterone receptor), epidermal growth receptor (EGFR or HER2) over expressed cancer and triple negative breast cancer (TNBC) that do not express any of these receptors means ER (-ve), PR (-ve) and HER 2 (-ve) as well [5]. The hormone responsive breast cancers are estrogen receptor positive (ER+), progesterone receptor positive (PR+) or both and among them majority of hormone-responsive breast cancer are ER+ (approximately 75%). Though, estrogen receptors are members of nuclear receptor super family; however, in cancerous conditions, they remain frequently present on cell surface as well [6]. These cell surface estrogen receptors are associated with the growth and proliferation of breast cancer. Such high level of expression of estrogen receptors has been widely exploited for targeted drug delivery as drug conjugates [7,8], as targeted nanocarriers [9,10] and also for gene delivery [11] to ER+ breast cancers. However, dual targeting of both nuclear ER and cell surface ER using specific drug delivery design is not reported till date.

Targeted nanoparticles have been widely explored for site specific drug delivery of chemotherapeutic agents with improved pharmacokinetics and lower systemic toxicity [12]. It is noteworthy that the properties of selected polymeric material for the preparation of such targeted nanoparticle play an important role as it affect not only the clinical performance of the delivery system but also affect the regulatory clearance at the time of translation of the product from bench to bedside. Chitosan, a natural biopolymer, is biocompatible, biodegradable, and safe material for the construction of nanoparticles. It offers modification opportunities due to the presence of several amino ($-NH_2$) group in its chemical structure that are resourceful for the tethering of various ligands and transforming it into a suitable carrier for biomedical application such as drug/gene targeting [13]. Doxorubicin (Dox) is one of the most popular and effective anticancer molecules commonly used in

* Corresponding author.
E-mail address: srai2k@gmail.com (S.R. Paliwal).

https://doi.org/10.1016/j.ijbiomac.2020.08.172
0141-8130/

breast cancer chemotherapy. However, its clinical use is associated with dose-dependent toxicities such as myelosuppression and cardiotoxicity. This may be turned up in to a clinically appreciable formulation based product using nanotechnological transformation altering improved efficacy and limiting side-effects [14].This is why a large number of drug-conjugates and Dox encapsulated carriers have been developed till date to achieve targeted Dox delivery and to circumvent its clinical side-effects [15].

Conventional methods of experimentation and optimization consider only one variable at a time and hence factor interactions cannot be determined. Recently, quality by design (QbD) has been recommended by ICH (Q8) guidelines to optimize the critical process parameters for getting the desired target quality in the product. Design of experiment (DoE) procedure commences with predetermined objectives and focuses on a better understanding of process parameters and product design. Further, DoE is used to correlate the relationship between independent variables (factors) and dependent variables (responses). DoE produces more reliable results with a lesser number of experiments with an added advantage of extrapolation of data by plotting the results. A response surface methodology has been explored to identify the response of independent variables for the optimization of pharmaceutical formulations. Among several design options, Box-Benhken design is the most commonly applied design with a minimum run of experiments [16].

Thus, considering all these aspects, we hypothesized to construct Es conjugated Dox incorporated chitosan-estrone nanoparticles (CSEsNPs) formulation further called as DoxEs-CSEsNPs in order to explore dual ER targeting at the nuclear and cellular level both. BBD design was applied to optimize the process parameters for the preparation of nanoparticles. Here, Dox-Es conjugate may play a dual role. First, when the conjugate is reached in the intracellular compartment of cancer cells, it will bind to ERs which carries Dox-Es towards the nucleus i.e., the site of doxorubicin action and hence may limit efflux of Dox. Second, Dox-Es, if leached from nanoparticles during transit in the blood pool; conjugated Dox-Es may navigate the Dox to the target site by protecting it from non-specific distribution to non-target sites. The Dox/DoxEs containing CSEsNPs preparations were investigated for different characterization parameters. The qualitative localization study was performed using fluorescence microscopy. Cytotoxic potential and targetability was assessed on MCF-7 cell lines. The developed formulations were also evaluated for in vivo performance on tumor-bearing rat model where various pharmacokinetic parameters were also determined.

2. Materials and methods

2.1. Materials

Chitosan (CS), estrone (Es), sodium tripolyphosphate (TPP), succinic anhydride (SA), dimethylaminopyridine (DMAP), N hydroxysuccinimide (NHS), dicyclohexylcarbidiimide (DCC), triethylamine (TEA), N-(3-dimethylaminopropyl)-N-ethylcarbidiimide (EDC) and dialysis membrane (MWCO 12–14 kDa) were purchased from Himedia, India. Doxorubicin was provided by Sun Pharma (Vadodara, India). All other reagents and solvent were either of analytical or HPLC grade.

2.2. Methods

2.2.1. Conjugation of Es with Dox

DoxEs conjugate was synthesized using the method described by Rai et al (2008) and Cao et al (2008) with some modifications [17,18] (Fig. 1A). Briefly, Es was activated using SA, for that Es (270 mg, 1 mmol), SA (150 mg, 1.5 mmol), DMAP (122 mg, 1 mmol), and TEA (139 μL, 1 mmol) were dissolved in dioxane, and the resulting solution was stirred (Remi 2-MLH) overnight at room temperature (RT). The dioxane was evaporated under vacuum (MAC New Delhi), completely and the residue was dissolved in a minimum quantity of DCM then filtered. The obtained filtrate was further concentrated and precipitated with cold diethyl ether and air-dried to yield carboxylic acid derivative of Es (i.e., Es-SA). Further, Dox containing -NH_2 group and COOH-estrone was conjugated with corbodimide chemistry using N,N′-DCC and N-NHS. Briefly, the Es-SA (40 mg, 0.1 mmol) was reacted with Dox (87 mg, 0.15 mmol) in the presence of DCC (61.8 mg, 0.3 mmol), NHS (34.5 mg, 0.3 mmol) and TEA (42 μL, 0.3 mmol) in DMSO at RT under nitrogen (N_2) atmosphere for 24 h. The product was filtered to remove N,N-dicyclohexylurea (DCU) and then lyophilized (Labconco 4.5 L, Freezone Plus cascade benchtop freez dryer, USA) to remove DMSO.

2.2.2. Conjugation of estrone with chitosan

To obtain Es conjugated CS (CSEs) polymer, an amidation reaction was applied as described by Guo et al., 2014 with slight modification [19]. Functionalized Es-SA as obtained earlier was conjugated with primary amine groups of CS by using NHS/EDC mediated carbodimide coupling reaction. The Es-SA (80 mg, 0.2 mmol), NHS (34.5 mg, 0.3 mmol) and EDC (57.5 mg, 0.3 mmol) were taken in anhydrous DCM for 24 h at room temperature under constant stirring (Remi 2-MLH). After evaporation of the solvent, the product was added into CS acetic acid solution (1% *v*/v, pH = 4). After 24 h the reaction was completed and the conjugate was dialyzed against distilled water for 72 h in order to remove free reactants and lyophilized (Labconco 4.5 L, Freezone Plus cascade benchtop freeze dryer).

2.2.3. Characterization of DoxES and CSEs conjugates

The conjugation of CSEs was confirmed by FT-IR (8400S, Shimadzu) and FT-NMR (Bruker's AVANCE-III, 500 MHz) spectroscopy for various shifts and peaks and interpreted for different groups.

2.3. Preparation of chitosan nanoparticles

Dox and DoxEs loaded chitosan nanoparticle was prepared by ionic gelation of CSEs with TPP with slight modification on our previously reported method Fig. 1B [20]. Firstly, CSEs was dissolved in acidic solution containing 1.0% (*v*/v) glacial acetic acid. Then pH of the solution was increased to 4.7 by adding 0.1 N NaOH. The TPP was added to the above solution with different CSEs/TPP ratio under constant stirring (Remi 2-MLH). After 1 h stirring, the solution was sonicated (PCiTM 3.5 L 100) and centrifuged (Remi, C-24) at 15000 rpm for 30 min on glycerol bed. The CSEs nanoparticles were collected at the bottom of the centrifuge tube as a transparent gel pellet. The pellet of chitosan nanoparticles was dried by a freeze dryer (Labconco 4.5 L, Freezone Plus cascade benchtop freez dryer, USA) before characterization. In order to get drug entrapment, the drug (Dox/DoxEs) was added in to the CSEs solution in glacial acetic acid before the addition of TPP solution.

2.3.1. Experimental design

For the optimization of formulation parameters, a 3-factor and 3-level Box-Behnken (BBD) design was employed using Design-Expert Software (Stat-Ease Inc., Minneapolis, MN). This design was selected because it requires only three levels of each independent variables and exploring quadratic response surfaces with second-order polynomial models suggesting the minimum number of experimental runs capable to indicate the variable interaction. It does not contain the extreme level of variables which may leads to difficulties with respect to formulation development and unsatisfactory results.

The independent variables were, (X_1) CSEs to TPP ratio, (X_2) sonication time and (X_3) the stirring speed, with 3 level viz., low level (−1), mid-level (0), high level (+1) respectively, while dependent variables were (Y_1) particle size and (Y_2) percent entrapment efficiency. Table S1 represents the level of these dependent and independent variables. Design matrix consisting of 17 experimental runs including five centre points was constructed. The computer-

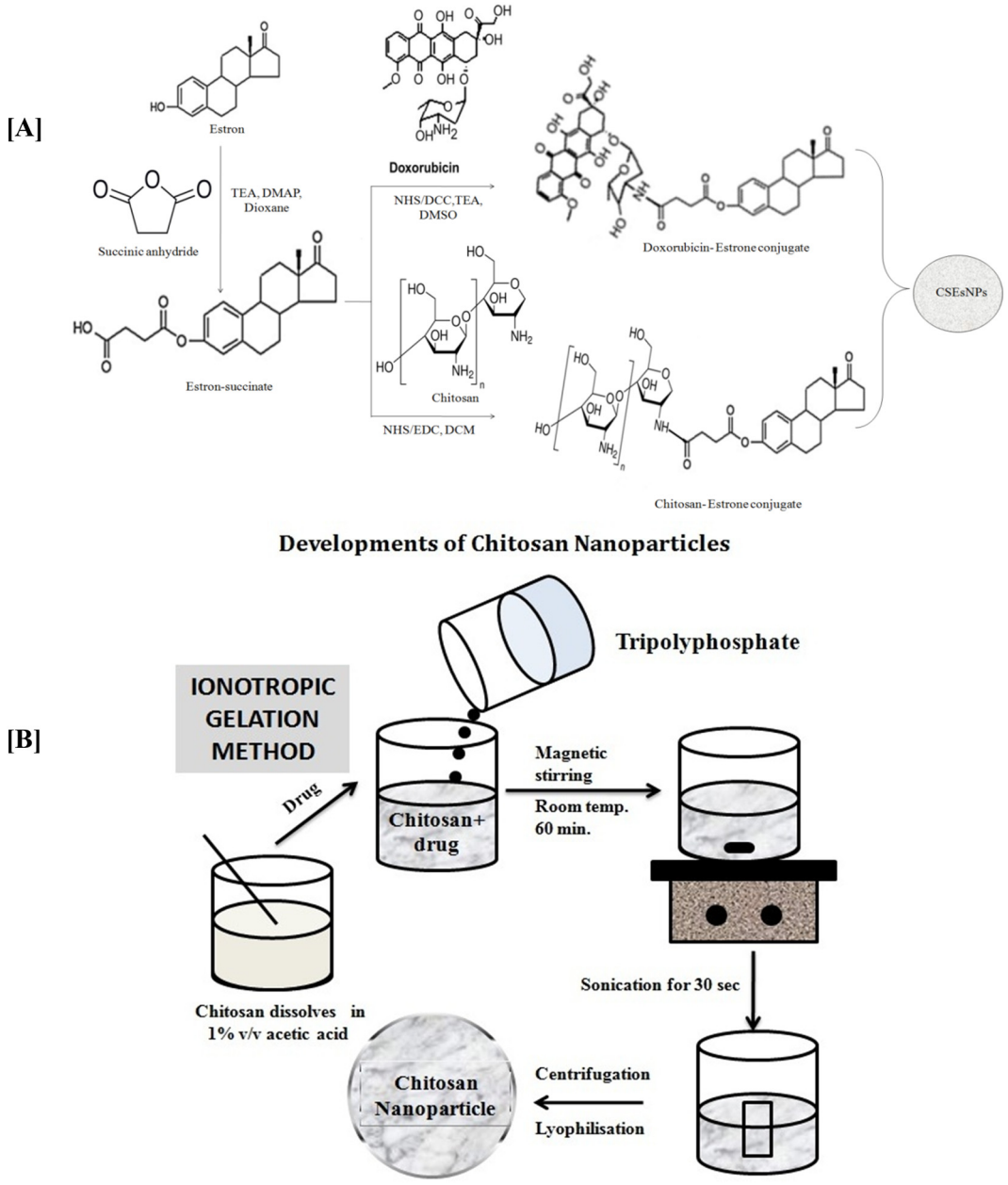

Fig. 1. [A] Schematic diagram demonstrating conjugation of estrone with Dox (DoxEs) and chitosan(CSEs); [B] Scheme of method of preparation of chitosan nanoparticles.

generated nonlinear quadratic model equation of the design is as follows:

$$Y = A_0 + A_1X_1 + A_2X_2 + A_3X_3 + A_4X_1X_2 + A_5X_2X_3 + A_6X_1X_3 + A_7{X_1}^2 + A_8{X_2}^2 + A_9{X_3}^2$$

where, A_0: the intercept representing the arithmetic average of all of 17 runs; A_1-A_9: the regression coefficient obtained from the results of experimental response to dependent variable Y; X_1, X_2, and X_3: are the independent variables; X_1X_2, X_2X_3, and X_1X_3 are the interaction terms which represents the effect on the response on a variation of two factors simultaneously; X_1^2, X_2^2, and X_3^2: quadratic terms.

Seventeen batches of CSEsNPs were formulated as suggested by design expert and the effect of factors on responses were evaluated (Table 1). The best-fitting model or the quality of the model was evaluated after considering different statistically parameters obtained by analysis of variance (ANOVA) like p value, coefficient of determination (R^2), percent coefficient of variance (% CV), predicted residual sum of squares (PRSS) etc. with the level of significance at $p < 0.05$. Response surface analysis applied for measuring the effect of the independent variables on formulation attributes. The resulted perturbation and 3D plots were critically observed for showing the direct effect and interactions which was considered for the selection of the experimental model. The effect of factors on responses was analyzed by BBD and optimization of the formulation was done to attain a lower particle size of NPs and higher percent entrapment efficiency using overlay graph.

2.3.2. Differential scanning calorimetry

Differential scanning calorimetry characterizations of CS, Es, CSEs, Dox, and DoxEs-CSEsNPs were carried out with differential scanning calorimeter (DSC 4000, PerkinElmer). Each sample was scanned between 40 °C and 350 °C and blank aluminium pans were employed as reference. The temperature of maximal excess heat capacity was defined as the phase transition temperature.

Table 1
Observed response obtained after performing the factorial runs given by BBD.

Runs	Factor 1	Factor 2	Factor 3	Response 1	Response 2
	A:CSEs:TPP	B:ST	C:SS	PS	EE
	% wt/wt	Sec	/Sec	nm	%
1	−1	0	1	366.42	66.24
2	0	−1	1	257.66	69.32
3	0	1	1	213.23	60.87
4	−1	0	−1	387.12	68.45
5	0	0	0	263.58	62.32
6	1	1	0	134.41	52.64
7	1	0	1	131.78	53.91
8	0	0	0	268.26	66.37
9	0	1	−1	196.32	61.12
10	−1	−1	0	394.54	69.35
11	−1	1	0	357.34	67.21
12	0	−1	−1	292.12	62.38
13	1	0	−1	169.98	57.82
14	1	−1	0	173.56	58.64
15	0	0	0	246.27	61.37
16	0	0	0	237.61	59.43
17	0	0	0	240.18	60.12

2.3.3. Determination of particle size, polydispersity index (PDI), zeta-potential and morphology of chitosan nanoparticles

The average particle size, PDI, and zeta potential of nanoparticles was determined on the basis of dynamic light scattering principle using Zetasizer (ZS90 zetasizer, Malvern Instrument, UK). All measurements were performed in triplicate at 25 °C.The morphology of CSEsNPs were examined by a high-performance digital imaging TEM (TECNAI 200 Kv TEM, Fei, Electron Optics). One drop of the suspended solution was spread onto a carbon-coated copper grid and stained with 2% (*w*/*v*) phosphotungstic acid. After drying at RT the samples were placed for TEM analysis using an accelerating voltage of 200 kV.

2.3.4. Determination of drug entrapment efficiency

Percent entrapment efficiency (EE) of Dox in CSEsNPs was estimated by an indirect estimation of free drug. The free unentrapped drug was removed after centrifugation by supernatant with the washing of nanoparticles at least four times for complete removal of free drug and estimated using UV spectrophotometer at λ_{max} 480 nm (UV-1800, Shimadzu).

2.3.5. In vitro drug release profile

The dialysis tube-based diffusion technique was used for the assessment of in vitro drug release behaviour of the formulations. Two-milliliter solution of the selected formulation was placed in the dialysis sac of benzoylated dialysis membrane (MWCO, 12–14 kDa, Himedia), hermetically tied, and immediately suspended in 20 mL of aqueous phosphate buffer saline (PBS pH 7.4) receptor medium. The sink condition was maintained in the receptor compartment through constant stirring using magnetic stirrer and withdrawing large samples (Remi 2-MLH) at 37 ± 0.5 °C. The Dox release was determined in withdrawn aliquot, after appropriate dilution, using UV spectrophotometer (UV-1800, Shimadzu).

2.3.6. Effect of pH on pharmaceutical characteristics

The pH of the biological mediums may affect the formulation characteristics. To evidence any such change, the effect of pH on the formulations was determined by measuring the particle size, zeta potential and PDI at various pH values using Zetasizer. The nanoparticles dispersion was incubated in 20 mM acetate buffer (pH 5.8 and 7.4) at 37 ± 1 °C up to 4 h and then observed at least three times for above parameters.

2.4. Haemolysis studies

Fresh human blood sample (1.0 mL) was collected into vials (HiAnticlot Vials Flat Bottom) and immediately centrifuged at 2000 ×*g* for 5 min leading to separate RBCs. Obtained RBC pellet was washed 3–4 times with normal saline solution and re-suspended into saline solution. Further, about 1.0 mL of the RBCs suspension was added to 1.0 mL of either of 0.01, 0.02, 0.03, 0.04, and 0.05%, *w*/*v* solution of different formulations (i.e., Dox, DoxEs, Dox-CSEsNPs, DoxEs-CSEsNPs), double distilled water (100% haemolysis) and normal saline (blank samples). These tubes were incubated for 1 h at 37 °C with gentle hand shaking. On completion of incubation, centrifugation was done for 5 min at 2000 ×*g*. The obtained supernatant was analyzed by UV–Vis spectrophotometer (UV-1800, Shimadzu) at λ_{max}415 nm as reported elsewhere [21].

2.5. Cytotoxicity studies

The cytotoxicities of the developed formulations were estimated using the MTT assay. The MCF-7 cells were treated with free Dox, DoxEs, Dox-CSEsNPs and DoxEs-CSEsNPs formulations at the equivalent concentration of Dox (1, 5 and 10 μg/mL). After 48 h, cell lines were exposed to MTT solution (20 μL, 5 mg/mL in PBS). These cells were washed after 4 h followed by addition of dimethyl sulfoxide to ensure complete dissolution of formed formazan crystals. The absorbance at 570 nm was measured using microplate reader (BIO-RAD, model 680, UK) comparing with untreated control cells. Percent cell viability was than determined at different concentrations. To study the role of estrogen receptor-mediated uptake a competitive binding in presence of free estrone was also performed. The cells were pre-incubated with estrone for 1 h before treatment with the formulations.

2.6. In vivo studies

The studies were performed in compliances with committee for the purpose of control and supervision of experiments on animal, Ministry of culture, Government of India and the study protocols were also approved by Institutional Animal Ethics Committee (Ref. No. 224/IAEC/Pharmacy/2018) Guru Ghasidas Vishwavidyalaya, Bilaspur, CG, India.

2.6.1. Blood level and biodistribution of Dox

Female rats (Spargue-Dawley, 40–45 days) were taken and kept under standard conditions and fed with laboratory food. After 10 days, DMBA in soyabean oil (65 mg/kg) was administered orally to induce breast cancer. Approximately after 3 months, tumor had developed in the animals. In vivo blood levels and biodistribution patterns were estimated on these tumor bearing animals. Briefly, tumor-induced animals were randomly distributed into five groups. The first group received saline and served as control. While second, third, fourth, and fifth group animals received free Dox, DoxEs, Dox-CSEsNPs, and DoxEs-CSEsNPs formulations respectively intravenously at the equivalent dose of Dox at 5 mg/kg body weight via tail vein injection. Animals were sacrificed at different time intervals for the collection of visceral organs such as heart, lungs, liver, kidney, and tumor immediately. The blood samples were also collected every time. Dox was then extracted from the collected tissues using methanol after homogenization. Amount of Dox was quantified in blood and organs/tissue by using a previously reported HPLC method (YL9100 HPLC) [22]. The data were normalized to tissue weight.

2.6.2. Qualitative estimation using fluorescence microscopy

The fluorescence microscopy was performed in female rats to confirm the accumulation of different Dox formulations. The selected nanoparticle formulations were injected in the tail vein of the rats. The treated rats were then sacrificed after 6 h and major organs tissue like heart, liver, lungs kidney, and breast were excised. These tissues were

treated, sectioned, and observed under inverted fluorescent microscope (Leica DM IL LED, Germany).

2.6.2.1. Histopathology analysis. Histopathology analysis was done to assess the effect of Dox on heart tissues. The different formulations were administered to the rats. The heart was collected, washed with saline and fixed with 10% formalin. After fixation, it was embedded in paraffin, sectioned and mounted on glass slides. The samples were stained with hematoxylin and eosin and observed under light microscope [23].

2.7. Statistical analysis

All data were expressed as mean ± SD and Analysis of variance (ANOVA) was applied for the comparisons among three or more groups followed by post hoc Tukey-Kramer test. Student's *t*-test was performed for comparison between two groups. For statistical significance $p < 0.05$ was considered for all comparisons.

3. Result and discussion

3.1. Conjugation and characterization of DoxEs and CSEs

Conjugation of Dox and Es was carried via primary amine group to the carboxylic group. An excess amount of Dox was introduced to achieve complete reaction with Es-SA. DoxEs was synthesized under two steps namely i) Activation of estrone by succinic anhydride to convert estrone into estrone succinate presenting -COOH group and ii) Conjugation of Dox and activated estrone (Es-Succinate) by amide bond formation with -NH_2 group of Dox and -COOH group of estrone succinate by carbodimide chemistry using DCC and NHS as coupling agents in DMSO. Chitosan and Es conjugate polymer (CSEs) was also synthesized by conjugating amino groups of CS and carboxylic group of Es-SA by using NHS/EDC as coupling agents. Estrone conjugated Dox and CS were characterized by IR and NMR spectroscopy. Different IR bands at 1712.79 cm^{-1}C=O (Ester), 3053.32 $cm^{-1}CH_2$ (Methylene), 1249.87 cm^{-1} C-O-C (Ester), 3018.6 cm^{-1} CH_3 (Methyl), 3585.67 cm^{-1} -OH (carboxylic acid), 1614.42 cm^{-1} Primary amide band; 3346.50 cm^{-1}, (N—H stretch); and 1583.56 cm^{-1}, (C—N stretch) are observed in the spectra. The peak at 1678.07 cm^{-1} (C═O stretch of CO-NH) confirmed the conjugation of Es-SA with Dox via amide linkage [18].

The IR spectrum of CSEs showed the stretching of -OH groups at 3344.57 cm^{-1} with broad peak because of the hydrogen bonds. The -OH band may be overlapping the stretching band of -NH. Two consecutive bands between 2900 and 2800 cm^{-1} represents the C—H symmetric and asymmetric stretching respectively. The presence of bands in between 1300 and 1200 cm^{-1} shows the ester (C-O-C) and amide (CO-NH) peaks respectively. The disappearance of characteristic stretching vibration of the amino group in conjugates and the presence of characteristic C═O bands of estrone around 1700 cm^{-1} confirm the CSEs synthesis [24,25].

The ^{1}H NMR spectra of DoxEs conjugate exhibited typical peaks at 3.633 ppm (H_3C-O-C-1), 5.625 ppm (HC-10), 6.887 ppm (HC-3) and 7.059 ppm (HC-2 and HC-4). The spectrum showed an intense peak at 2.984 ppm, which characterize the methylene protons of the Es. Shift at 7.039 ppm helps to distinguish the -CONH amide group of conjugated system. ^{1}HNMR spectra of CSEs also showed all characteristic proton peaks of CS and Es. There was a chemical shift in the CS and Es peaks due to a steric effect. The shifted peak assignments were found at 5.625 for aromatic -OH and 8.006 for -NH *sec* amide of conjugates. Chemical shift at 4.852 ppm for C-1 and at 3.976 ppm for C-2 observed respectively. As suggested earlier, the spectrum of CSEs also showed an intense peak at 2.983 ppm, which is the characteristic of methylene protons of the Es and shift at 7.054 ppm helps to distinguish the -CONH amide group of the conjugated system [17,21].

3.2. Preparation of chitosan nanoparticles

Chitosan nanoparticles can protect the trapped drug from proteolytic degradation and offers a selective intracellular targeting for the loaded drug in a passive/active manner. CSNPs were prepared by a well-established ionic gelation method, which consists the ionic interaction between positively charged amino groups (-NH_3^+) of CSEs and the negatively charged phosphate groups (-$P_3O_{10}^{5-}$) of TPP at acidic pH [26].

3.3. Optimization and statistical analysis of experimental data

Box-Behnken Design (BBD) was used for the optimization of process parameters. It provided generous-sized valuable information and proclaimed the value of statistical design for carrying out experiments. The selected independent variables like the ratio of CSEs to TPP, sonication time, and stirring speed played a critical role in the development of NPs with influence on the observed responses for particle size (PS) and % entrapment efficiency (EE). The three factors, three levels BBD with 17 runs experimental design were performed to assess the effect of independent variables on the observed responses. Different variables practical data were analyzed with Design-Expert software based on the constrained condition of desirability (Table 1) and quadratic polynomial equations generated by ANOVA were statistically validated to set-out the fitness of model and of the different variables. The selected independent variables like the ratio of CSEs to TPP, ST, and SS played a critical role in the development of NPs with influence on the observed responses for PS and EE. Polynomial equations point out the main and interaction effects which were determined by the assessment of statistical parameters. The positive or negative sign for the values in polynomial equations coefficient describe the positive effect or negative effect respectively of independent variables on the responses in quadratic equation. The quadratic model considered best fitted and highly significant on the basis of F value (>0.001). The *p*-value <0.05 was considered statistically significant for this model. The insignificant lack of fit value (>0.05) applied for the prediction of the model. The ratio of the explained variation and total variation for the responses known as the coefficient of determination (R^2) was used for the determination of the degree of the fit model (≈1) along with the maximum $_{adj}R^2$ which also explains the suitability of design and increase with the introduction of new variables only. The difference between R^2 and$_{adj}R^2$ should be resided in less the 0.2 for the conclusion of the goodness of the model. The reproducibility of the model expressed as percent coefficient of variance (% CV) is a ratio of the standard error of the estimate and observed response mean. The % CV deliberate for the purpose of reproducibility and below 10% of CV can be considered for reproducible model [27,28]. ANOVA fit statics presents another parameter called as adequate precision used to measures the range in predicted response and its associated error or called signal to noise ratio (> 4 considered as desirable value). Additionally, the sum of squares (SS) for each independent variable ascribed the model to analyze the percentage contributions of the same. Perturbation plots and response surface 3D plots were used for observation of the effects of the predetermined factors on the response i.e. PS and EE based on the model polynomial functions, to determine the change in the response surface (Figs. S1 & S2). The steep and curvature slope structure of the graph is known for the sensitive response change with that particular factor, whereas comparatively, flat line indicated the insensitivity of independent variables over the response. The perturbation graph is useful to observe the most affective variables for that response. These plots infer the role of each variable on each response which can be perceived by the developed formulations. Additionally, the check point optimized formulations were also used to confirm the magnitude of independent variables predicted by the generated equation for validity evaluation of model.

3.3.1. Analysis of responses

Seventeen trials of CSEsNPs were formulated in accordance with BBD and were fitted into the experimental design provided by the Design-Expert software. Table 1 represents the influence of independent variables on responses.

3.3.1.1. Response Y_1 (particle size). Transformation of data assumed as an important factor in statistical analysis. Further, the maximum to minimum ratio of practical value for dependent variables Y_1 was found 2.99 which suggested no power transformation required. The transformation of response plays a vital role in data analysis. Transformation is essential if the error (residuals) is a function of the magnitude of response (predicted values). The thumb rule of power transformation in responses is necessary. The thumb rule of power transformation responses is when ratio of maximum to minimum response is greater than 10 transformations is not required, whereas less than 3, transformation is required.

ANOVA calculations measure the effects of concentration of CSEs to TPP ratio, ST, and SS on the response PS. The suitability of the model for the analysis of the independent and dependent variables was done on the basis of, lack of fit (F value 1.26) and the Prob > F value of $p < 0.0001$, low SD, high R^2, and lower PRESS value, which suggested quadratic model for Y_1 response (Table S2).The ANOVA statistical data calculation confirms significant model on the basis of (Prob > F less than 0.0001) along with F value for response (Y_1 was 56.44). Lack of fit F value PS suggested that lack of fit was not significant relative to the pure error. The various multiple regression terms i.e. ${}_{pred}R^2$ and ${}_{adj}R^2$ values for PS were in good agreement i.e. 0.9689 and 0.8835, respectively and indicated that the predicted responses are good and fit to the model. Additionally, adequate precision (24.715) determined the signal-to-noise ratio desirable (>4). The obtained quadratic model is utilized to find the experimental design space.

Obtained quadratic equation for Y_1 (PS)

$$\begin{aligned} PS\ (Y_1) = {} & 251.18 - 111.961 \times {}_1 - 27.0725 \times {}_2 - 9.55625 \\ & \times {}_3 - 0.4875\, X_1X_2 - 4.375X_1X_3 + 12.8425X_2X_3 + 18.8875 \\ & \times {}_1{}^2 - 5.105 \times {}_2{}^2 - 6.2425 \times {}_3{}^2 \end{aligned} \quad (1)$$

The regression equation indicates the effect of all the three formulation variables (X_1, X_2 and X_3), where X_1, X_2, and X_3 are the main effects influencing the response Y_1. The X_1 X_2, X_1 X_2, X_2 X_3, X_{12}, X_{22}, and X_{32} are the interaction terms phrases with second-order factors which stand for the nonlinear relationship between the dependent variables and the independent variable and showed that the PS was changing when two independent variables were altered simultaneously. The quadratic equation positive and negative sign are magnitude of independent variables synergistic and antagonistic effects, respectively on the response. The quadratic equation for PA suggested the negative effect of CSEs to TPP ratio, ST and SS. Apart from this, from perturbation graphs obtained, the influence of individual independent factors on the PS was also observed (Fig. S1). For response Y_1, Factor A (CSEs:TPP) was showing vertical slope line which implies that the CSEs to TPP ratio was most influencing for PS. Additionally, factor B (ST) and factor C (SS) provided noticeable slope and slight bend respectively suggesting somewhat less effect than CSEs:TPP. It is evident that the concentration of TPP increased the PS significantly possibly due to high anion interaction with positively charged CSEs ions. On increasing concentration of CSEs, the particle size of NPs increased but opposite to TPP effect, the ZP of NPs also increased due to the positive charge of CSEs. During the stirring, high shearing forces reduces the particle size but it also increases the surface energy and aggregates forms to reduce this energy by reducing the surface area. However, sonication energy breaks the aggregates and the particle size further decreased. The strong negative coefficient of all three main factors indicates that particle size is inversely proportional to all the studied variables. This was in agreement with our earlier reported studies [20].

Table 2
Optimized process parameters of Box-Behnken design.

Level	CSEs:TPP (ratio)			ST(sec)			SS		
	−1	0	+1	−1	0	+1	−1	0	+1
Parameters level	1:1	2:1	4:1	60	90	120	Slow	Medium	Fast
Optimized magnitude	0.399			−0.842			0.999		
Optimized process parameters	1.6:1			75			Medium		

The mathematical relationship between the independent variables and the responses was expressed using the response surface plots. The interaction effect of X_1 and X_2wasanalyzed by keeping X_3 constant; the interactions effect of X_1 and X_3 was analyzed by keeping X_2 at constant level; and the effect of X_2 and X_3 and their interaction was studied when X_1 was kept at fixed level, on response Y_1respectively (Fig. S2[R_1-R_3]). When we increased the magnitude of X_1 and X_2 simultaneously, a negative effect on the particle size was observed (coefficient of $X_1X_2 = -0.4875$) as presented in Fig. S2 (R_1). The X_1 and X_3, also showed the same response with coefficient of X_1 $X_3 = -4.375$ (Fig. S2 (R_2)). The interaction effect of X_2 and X_3 variable on PS was less significant (coefficient of X_2 X_3 = $12.8425X_2X_3$) on the PS as shown in Fig. S2(R_3) where X_2 showed negative relationship while X_3 has no major effect over the Y_1.Particle size of the NP is the deciding factor which influences the drug release, bioavailability and efficacy of the formulations. Nanoparticles undergo cellular internalization by endocytosis; here PS has inverse relationship on cellular drug uptake and influence the drug bioavailability.

3.3.1.2. Response Y_2 (% entrapment efficiency). The maximum to minimum ratio was found to be 1.31 for the Y_2 response so power transformation is not required similar to Y_1 response. Quadratic model was suggested for the Y_2 response for analyzing it on the basis of lack of fit value, and other model summary statistics. The Prob > F value of $P < 0.0183$, low standard deviation, high R^2 and lower predicted residual error sum of square (PRESS) values. The data of ANOVA (Table S3) suggested the model was found significant (Prob > F is less than 0.05). The Model F value for response Y_2 was 5.41, which defines the model was significant. Magnitude of CSEs to TPP ratio, were significant model terms that influence the Y_2 response ($P < 0.05$). Lack of fit F value for Y_2 was 0.49 which implies that lack of fit was not significant relative to the pure error. The ${}_{pred}R^2$ and ${}_{adj}R^2$ values for response Y_1 were 0.6742 and 0.7637, respectively. This indicates that ${}_{pred}R^2$ value and ${}_{adj}R^2$ value are in good agreement indicating a good fit. Adequate precision for response Y_2 was 61.503 indicates that it is an adequate signal.

The generated quadratic equation for Y_2 (EE)

$$\begin{aligned} EE = {} & 61.922 - 6.03 \times {}_1 - 2.23125 \times {}_2 + 0.07125 \\ & \times {}_3 - 0.965X_1X_2 - 0.425X_1X_3 - 1.7975X_2X_3\ 0.88975 \times {}_1{}^2 \\ & + 0.92775 \times {}_2{}^2 + 0.57275 \times {}_3{}^2 \end{aligned}$$

The regression equation of response Y_2 showed negative relationship with CSEs to TPP ratio and ST but positive relationship with SS formulation variables. As evidenced by the negative regression coefficient for X_1 and X_2 in quadratic equation, CSEs to TPP ratio and ST was the major factor influenced the (Y_2) EE. A possible explanation may be that, ST may provide high energy for aggregation of NPs which leads to increased size CSNPs and EE as well. The perturbation graphs for response Y_2 (EE), factor A and B show steep curvature, whereas factor C showed slight curvature. It indicates that CSEs to TPP ratio and ST was important for determining EE. The 3D response surface graphs (Fig. S2 R'_1-R'_3) were articulated the mathematical relationship b/w the factors on the responses. It can be concluded from these plots that the two

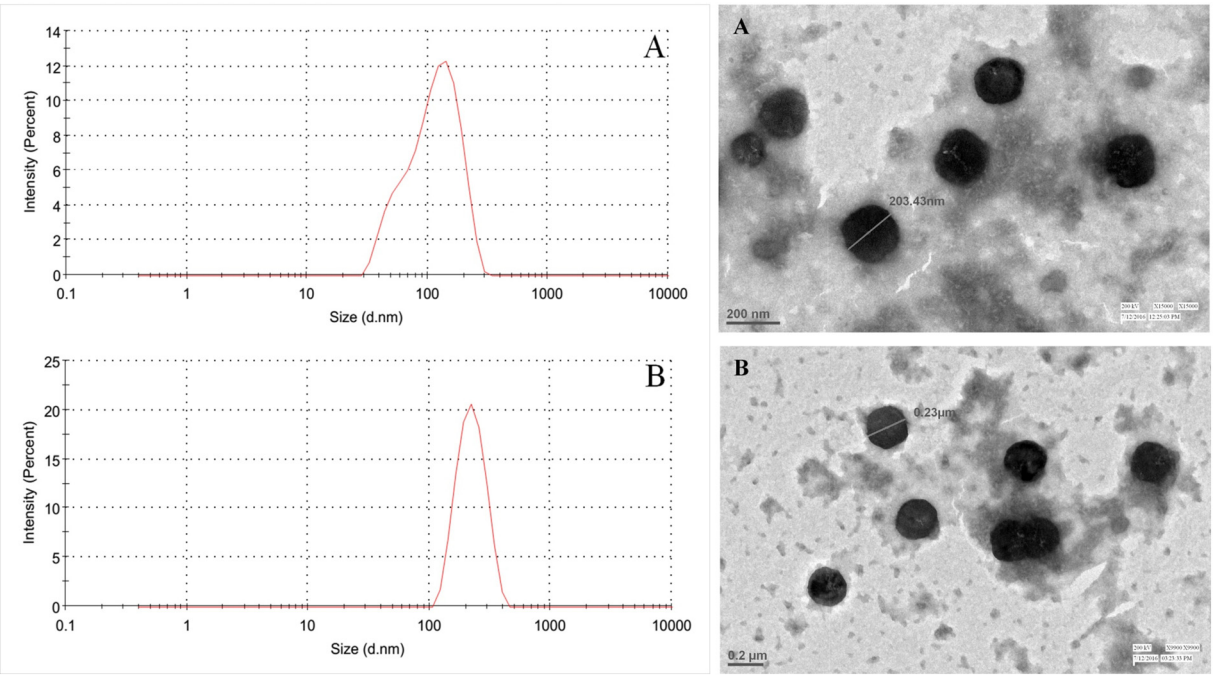

Fig. 2. Particle size distribution and TEM Photomicrograph of (A) Upper left and right Dox-CSEsNPs and (B) Lowe left and right DoxEs-CSEsNPs respectively.

variables are negatively influencing the response Y_2, and third one have positive effect may arise due to stirring energy provide more loading of drugs. The negative regression coefficient for simultaneous increase of X_1 and X_2 designated that the CSEs to TPP ratio and the ST had an inverse relationship with the EE.

3.3.2. Optimization and validation

The optimization of response i.e., PS and % EE with desirability as functions was undergone simultaneously. The overlay plot was plotted to acquire the optimized formulation conditions. The optimum formulation developed according to the set criteria of minimum PS to maximum %EE. Thereby, another batch of CSEsNPs with the predicted value of the formulation factors was prepared to validate the optimization protocol. The parameters of optimized formulation were 2:1 CSEs to TPP ratio, 30 s ST and medium SS which attains the requirements of optimization. The predicted value for PS and EE was 200.49 nm and 64.22% as shown in overlay plot respectively (Fig. S3). The optimized CSEsNPs formulation showed 199 ± 3.25 nm PS and 65.5 ± 1.95% EE, which was in good harmony with the predicted values. The desirability was found to be 0.911 (Table 2 and Fig. 3). The dependent variable (i.e. PS and EE) predicted value was found 200.49 nm and 64.22% respectively as shown in overlay plot. Conclusively the both obtained values were found in good harmony and close to each other.

3.4. DSC and TEM characterization

Different thermograms of CS, Es, Dox, CSEs, and DoxEs-CSEsNPs were obtained and are shown in Fig. S4. Dox has shown the solid-liquid transition at 202–204 °C in addition partially superimposed by an endotherm due to decomposition at 245 °C and this was continued to higher temperature [29]. Pure Dox and Es showed the sharp melting endothermic peaks at 202.35 °C and 266.73 °C respectively, which indicate crystalline nature of both the components. Polymer CS has shown peak at a temperature of 88.73 °C; whereas CSEs has shown peaks at 77.73 °C and 264.39 °C. This clearly suggested the conjugation of Es with CS. However, DoxEs-CSEsNPs formulation showed no sharp endotherm, suggesting decrease in crystallinity of Dox and Es which can be attributed to the fact that drug can be molecularly dispersed into the polymer matrix [30]. A minor peak at the area where Dox and Es present also suggested the compatibility between the drug and the polymers as well as reduction in sharpness of the peaks strengthen the entrapment of drug [31]. TEM images also confirmed about the morphological uniformity with almost homogenous shading of developed nanoparticles suggesting the compact structure of NPs formulations (Fig. 2).

3.5. Determination of pharmaceutical characteristics

As per Box-Behnken Design runs, selected formulation parameters were used to prepare CSEsNPs as described above. The formulations were characterized for different pharmaceutical parameters such as PS, PDI, ZP and SM. The average particle size of Dox-CSEsNPs and DoxEs-CSEsNPs were found to be 198.2 ± 14.3 nm and 206.4 ± 15.1 nm respectively (Fig. 2). The significant increase in the PS of DoxEs-CSEsNPs was observed as compared to Dox-CSEsNPs, this might be due to the entrapment of Es conjugated Dox which is lipophilic and may be less cationic in nature as compared to Dox. Polydispersity index (PDI) of Dox-CSEsNPs and DoxEs-CSEsNPs were found to 0.159 ± 0.012 and 0.166 ± 0.017 with ZP +30.6 ± 2.4 mV and +28.3 ± 2.8 mV respectively. ZP is essential to determine the stability of the colloidal preparation. The high ZP values play important role in stabilizing the formulations due to high repulsive forces, which hinders aggregation nanoparticles [32]. Percent drug entrapment efficiency for both formulations was found 66.33 ± 2.82% and 62.25 ± 2.63%

Table 3
Optimized pharmaceutical characteristics of the targeted nanoparticles.

Formulation code	Average particle size (nm)	PDI	Entrapment efficiency (%)	Zeta potential (mV)
Dox-CSEsNPs	198.2 ± 14.3	0.159 ± 0.012	66.33 ± 2.82%	+30.6 ± 2.4 mV
DoxEs-CSEsNPs	206.4 ± 15.1	0.166 ± 0.017	62.25 ± 2.63%	+28.3 ± 2.8 mV

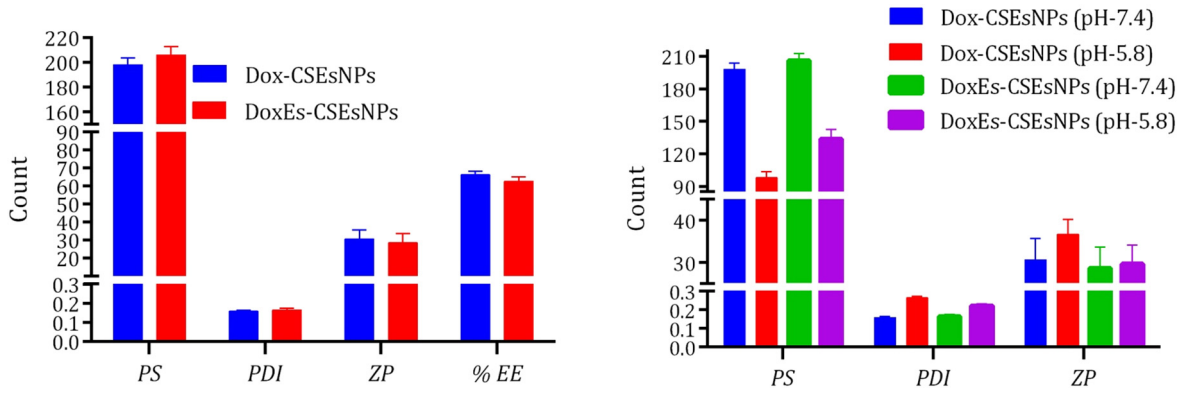

Fig. 3. Effect of pH on characterization parameters of Dox-CSEsNPs and DoxEs-CSEsNPs (mean ± SD, $n = 3$).

respectively (Table 3). This association of Dox and chitosan nanoparticles might occur due to possible hydrophilic interaction between NH_2 group of chitosan and OH and NH_2 group of Dox. However, the notable difference in EE might be due to lipophilic nature and molecular size of DoxEs conjugates different from plain DOX.

3.5.1. Effect of pH on characterization parameters of Dox-CSEsNPs and DoxEs-CSEsNPs

Fig. 3 shows effect of pH on various formulations. Both the formulations get slightly reduced in particle size at acidic pH (i.e. pH 5.8) due to CS solubility at acidic environment and this may be exploited for the desired drug release at acidic tumor microenvironment. Simultaneously, zeta potential and PDI were also increased due to positive charge and solubilisation of chitosan at this pH.

3.6. In vitro drug release profile

The release profiles of Dox-CSEsNPs and DoxEs-CSEsNPs formulations were performed at physiological pH 7.4 (37 ± 0.5 °C) using dialysis method. The obtained in vitro release pattern of both the formulations is shown in Fig. 4. The obtained results showed that the Dox release was higher approximately 30.87 ± 1.4% and 26.5 ± 0.98% for both Dox-CSEsNPs and DoxEs-CSEsNPs formulations respectively in the initial hours (3 to 5 h) reflecting a burst release of the drug. The burst release may be due to some surface adsorbed drug or may be due to entrapment of the drug in outer stratum of the nanoparticles. After 8 h, the drug release rate was observed comparatively slower and sustained for 72 h. The approximate drug release from Dox-CSEsNPs and DoxEs-CSEsNPs after 72 h was 82.7 ± 1.3% and 77.0 ± 1.2% respectively. The existing biphasic drug release behaviour is also supported by several research groups [33–36]. However, conjugation of Dox with Es decreased drug release that could be owing to structural veracity offered by the coupling of Es, and lipophilic nature which might result into dual barrier effect for Dox diffusion. In vitro release results of Dox-CSEsNPs and DoxEs-CSEsNPs formulations were further analyzed after treating data in different kinetic models such as zero- order, first-order, Korsmeyer-Peppas, Higuchi, and Hixson–Crowell. Both formulations Dox-CSEsNPs and DoxEs-CSEsNPs best-fitted in Higuchi model ($R^2 = 0.964$ and 0.961) as compared to other models, on the basis of obtained values of regression coefficients for various kinetics models (Table S4). The developed formulations were best fitted to Higuchi model that depict the diffusion controlled release behaviour [37].

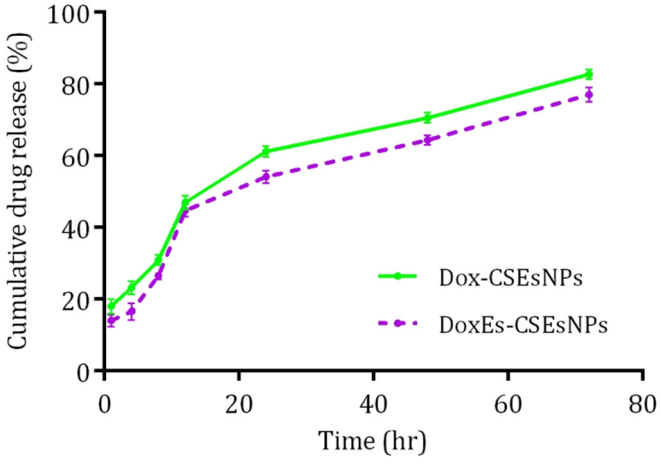

Fig. 4. In vitro drug release profile of Dox-CSEsNPs and DoxEs-CSEsNPs formulations (mean ± SD, n = 3).

3.7. Haemolysis studies

As expected among all the tested formulations, plain Dox was found to possess maximum haemolytic activity while DoxEs-CSEsNPs has shown negligible haemolytic activity. In all the cases, haemolytic activity was concentration-dependent. Plain Dox has high haemolytic activity (4.64 ± 0.208) at a concentration of 0.05% *w/v* in comparison to final formulation of DoxEs-CSEsNPs (1.3 ± 0.1) at similar concentration of Dox. These results of haemolytic toxicity of Dox matched with the earlier reports available in literature [38,39]. Conjugation of Es to Dox also reduced the haemolytic toxicity of Dox; this was further drastically reduced via the incorporation of conjugate in CSEsNPs due to masking of direct action on RBCs (Fig. 5).

3.8. Cytotoxicity studies

Cytotoxic potential of Dox, DoxEs, Dox-CSEsNPs and DoxEs-CSEsNPs was determined against MCF-7 cell lines. Results depicted that cell viability in all the four tested formulations, i.e., DoxEs, Dox-CSEsNPs, DoxEs-CSEsNPs and free Dox was concentration-dependent (Fig. 6). IC_{50} value of free Dox solution was higher than DoxEs-CSEsNPs, Dox-CSEsNPs and DoxEs. All nanoparticles based Dox formulations showed comparatively low IC_{50} value (i.e., $IC_{50} < 10$ μg/mL), however, DoxEs-CSEsNPs had significant higher cytotoxicity than DoxEs, Dox-CSEsNPs and free Dox solution. This effect may be attributed to the incorporation of Es in nanoparticles which enhanced cellular uptake, via receptor-mediated internalization by the cells [40]. This was further confirmed by performing competitive study after pre-incubation of cells with free ligand i.e. Es. Higher cell viability (%) was observed when Es was incubated prior to treatment with DoxEs-CSEsNPs, Dox-CSEsNPs and DoxEs. From these results, it is confirmed that the cytotoxicity of these Es tethered NPS was reduced due to saturation of receptors by free ligand and higher cytotoxic effect of DoxEs-CSEsNPs and Dox-CSEsNPs were attributed to its receptor-mediated endocytosis. The estrone conjugation with Dox might have contributed to lower IC_{50} value. DoxEs-

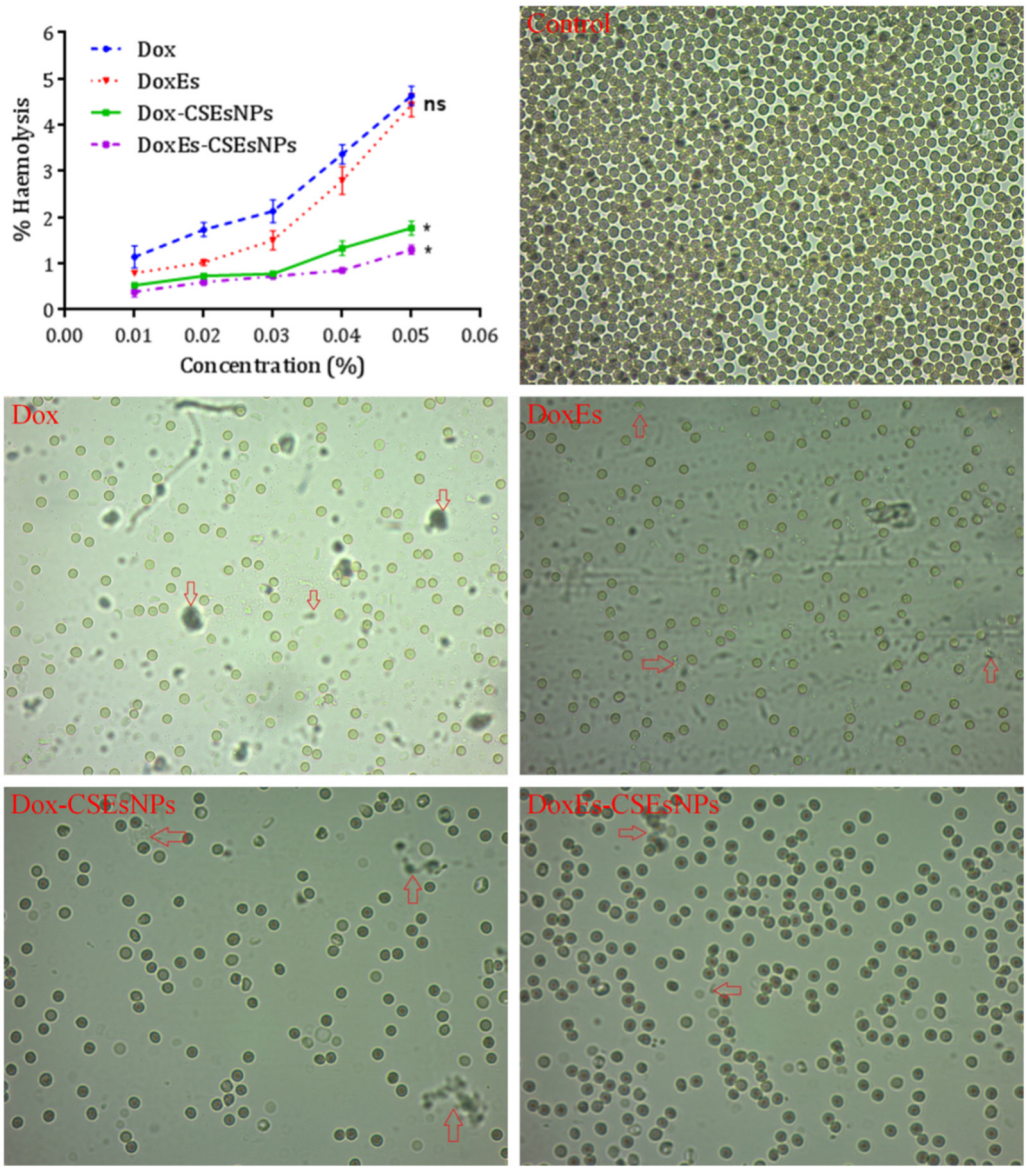

Fig. 5. Comparative studies of percent haemolysis of various formulations (10×).

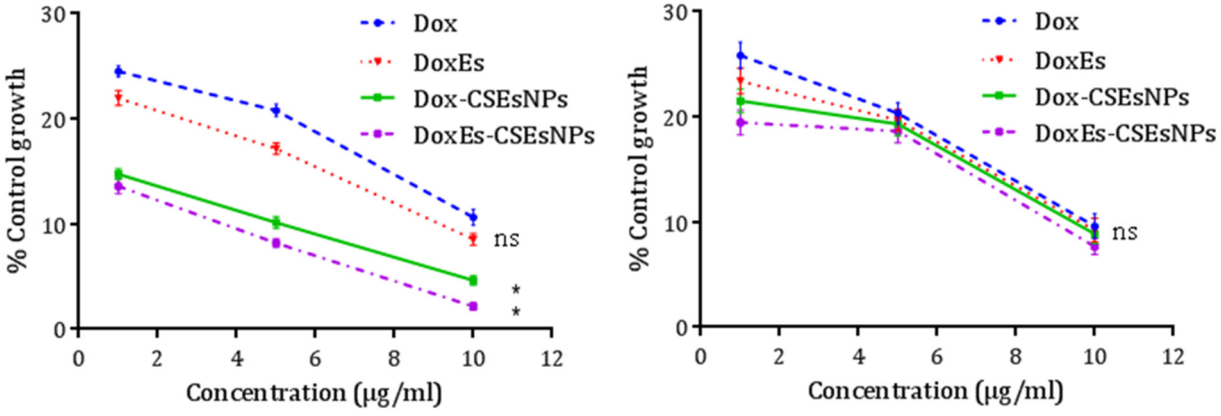

Fig. 6. In vitro cytotoxic activity of Dox, DoxEs, Dox-CSEsNPs and DoxEs-CSEsNPs using the MCF-7 cell at different concentrations after 48 h (mean ± SD, n = 3); Left; in absence of estrone; Right; in presence of estrone.

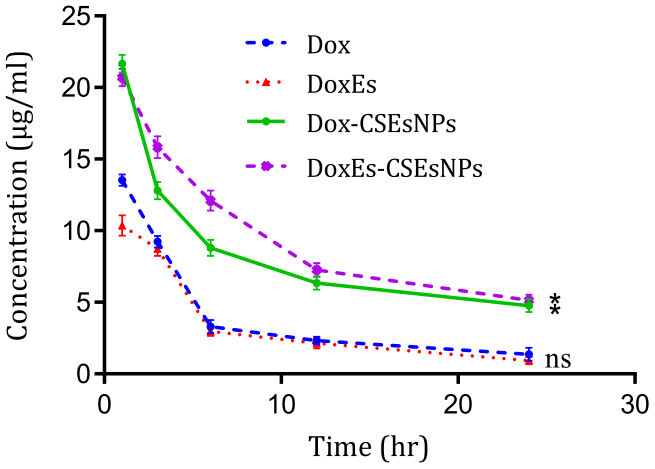

Fig. 7. Plasma concentration profiles of Dox after tail vein intravenous administration of free Dox, DoxEs, Dox-CSEsNPs and DoxEs-CSEsNPs formulations (mean ± SD, n = 3).

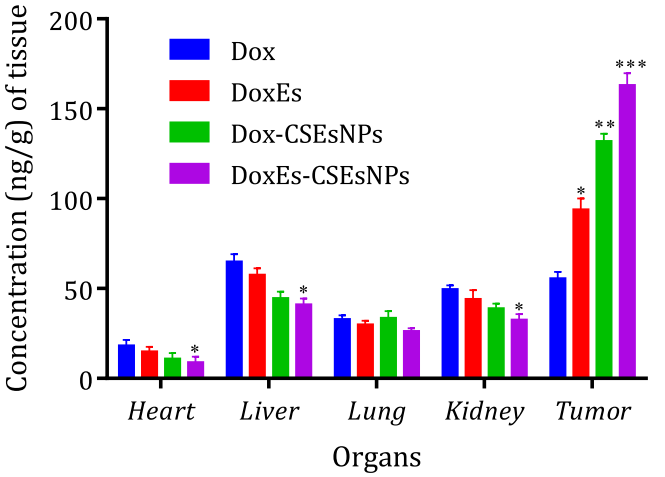

Fig. 8. Organ distribution profile of Dox, DoxEs, Dox-CSEsNPs and DoxEs-CSEsNPs formulations (after 6 h), Statistical significance compared with DoxEs-CSEsNPs group: $^{*}p < 0.05$, $^{**}p < 0.01$, $^{***}p < 0.001$ and ns = non-significant.

CSEsNPs showed higher uptake than Dox-CSEsNPs owing to receptor-mediated endocytosis by the MCF-7 cell lines. This might explain the higher toxicity of DoxEs-CSEsNPs than DoxEs, Dox-CSEsNPs and free Dox solution.

3.9. In vivo studies

3.9.1. Blood level studies

Blood level studies of Dox DoxEs, Dox-CSEsNPs and DoxEs-CSEsNPs were assessed to determine the release and performance of formulations in vivo. The formulations were centrifuged to remove unentrapped drug and drug concentration equivalent to that of free drug (5 mg/kg body weights) was administered to the female rats by i.v. route. The blood plasma was used to determine the concentration of Dox in blood samples at various time intervals.

The blood levels of Dox after administration of DoxEs-CSEsNPs, Dox-CSEsNPs, DoxEs and free Dox after 1 h were found to be 20.7 ± 0.34, 21.6 ± 0.35, 10.3 ± 0.40 and 13.5 ± 0.23 µg/mL, and after 6 h, 12.1 ± 0.70, 8.8 ± 0.55, 2.9 ± 0.30 and 3.3 ± 0.45 µg/mL, respectively. Free Dox and DoxEs were cleared rapidly from the circulation. About 1.3 ± 0.11%and 1.7 ± 0.09% of the injected dose was present in the blood after 24 h in respective cases (Fig. 7). Pharmacokinetic parameters of Dox-CSEsNPs and DoxEs-CSEsNPs formulation showed clearance from the blood with an elimination rate constant (K_{ele}) of 0.0575 ± 0.006 $h^{-1}$and 0.0590 ± 0.004 h^{-1} respectively (Table 4). However, in the case of DoxEs and free Dox the K_{ele} were obtained 0.1021 ± 0.041 h^{-1} and 0.0933 ± 0.012 h^{-1} respectively. AUC values for the blood drug concentrations from Dox-CSEsNPs and DoxEs-CSEsNPs were 280.585 ± 9.17 µg-h/mL and 317.729 ± 9.98 µg-h/mL compared to 89.167 ± 5.76 µg-h/mL and 107.044 ± 6.58 µg-h/mL values for DoxEs and free Dox, respectively. AUC results suggested the sustained release of drug from Dox-CSEsNPs and DoxEs-CSEsNPs formulation in vivo. In vitro release study also supported these results. The half-life ($t_{1/2}$) of Dox-CSEsNPs and DoxEs-CSEsNPs were 12.036 ± 0.126 h and 11.749 ± 0.981 h respectively and were significantly greater than the half-life of DoxEs(6.778 ± 0.764 h) and free Dox(7.419 ± 0.832 h) respectively. This may be due to slow and sustained release of drug from NPs formulation. The half-life was increased almost doubled using Dox-CSEsNPs and DoxEs-CSEsNPs than DoxEs conjugate and free Dox. Overall, increased $t_{1/2}$ and AUC, and decreased elimination rate remain constant in the case of NPs as compared with the free drug and therefore would be in favour of better efficiency of the drug.

3.9.2. Quantitative biodistribution of Dox in different organs/tissues

The quantitative estimation of drug concentration in various organs like heart, liver, lungs, kidney, and tumor after i.v. administration of free Dox at 6 h time interval showed maximum accumulation of the drug in non-target organs. Dox concentration after 6 h of i.v. administration in various tissues were 18.3 ± 3.0 ng/g in the heart, 65.1 ± 4.0 ng/g in the liver, 33 ± 2.0 ng/g in the lung, 49.6 ± 2.0 ng/g in the kidney, and 55.6 ± 3.5 ng/g in the tumor. The formulations DoxEs, Dox-CSEsNPs and DoxEs-CSEsNPs have shown different biodistribution profile in comparison to free Dox. These formulations were more accumulated in the breast tumor than other organs (Fig. 8). The drug recovered from the tumor in case of DoxEs-CSEsNPs (163.3 ± 6.4 ng/g) was significantly higher than free Dox (55.6 ± 3.5 ng/g, $p < 0.001$), DoxEs (94 ± 6.0 ng/g, $p < 0.001$) and Dox-CSEsNPs formulation (132.2 ± 4.0 ng/g, $p < 0.01$) in 6 h. The results clearly showed that there were approximately 3, 1.7- and 1.2-fold increase in tumor uptake in case of DoxEs-CSEsNPs formulation as compared with free Dox, DoxEs and Dox-CSEsNPs formulations respectively. The increased uptake of DoxEs-CSEsNPs may be due to the quick ERs recognition and internalization by the cell membrane of tumor tissue similar to our previous reports [10,41].

Table 4
Results for various pharmacokinetic parameters of different Dox formulations.

Parameters	Formulation code			
	Dox	DoxEs	Dox-CSEsNPs	DoxEs-CSEsNPs
Elimination rate constant K_{el} (h^{-1})	0.0933 ± 0.012	0.1021 ± 0.041	0.0575 ± 0.006	0.0590 ± 0.004
AUC (µg-h/mL)	107.044 ± 6.58	89.167 ± 5.76	280.585 ± 9.17	317.729 ± 9.98
V_d (L)	0.901 ± 0.034	0.988 ± 0.041	0.557 ± 0.023	0.480 ± 0.0039
Cl (L/h)	0.084 ± 0.0042	0.100 ± 0.0054	0.032 ± 0.0013	0.028 ± 0.002
$t_{1/2}$ h^{-1}	7.419 ± 0.832	6.778 ± 0.764	12.036 ± 0.126	11.749 ± 0.981

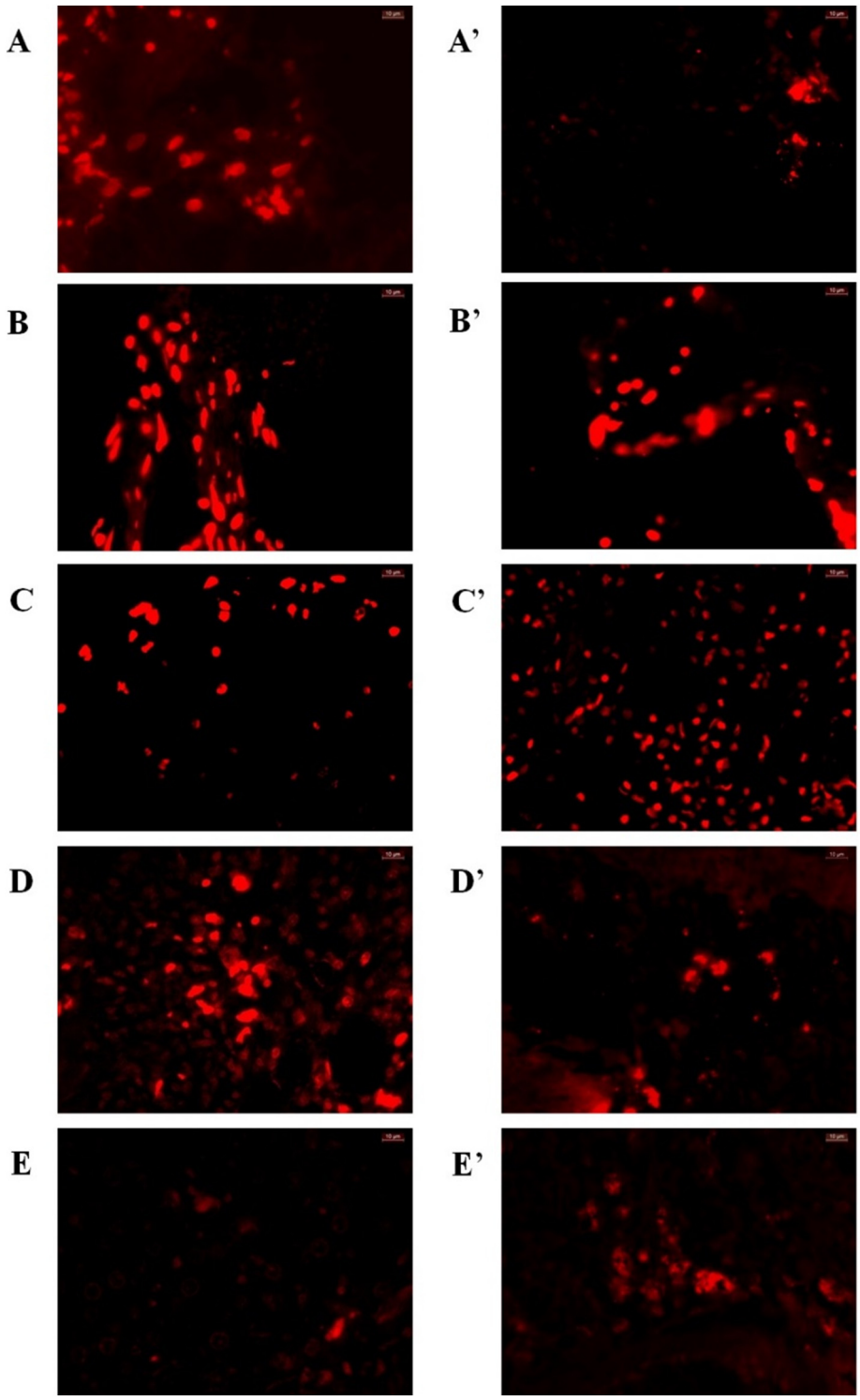

Fig. 9. Fluorescent photomicrograph of biodistribution (450×) after 6 h of tail vein intravenous administration of Dox-CSEsNPs and DoxEs-CSEsNPs, respectively. (A & A′) Heart (B & B′) Liver (C & C′) Lung, (D & D′) Kidney and (E& E′) Tumor.

3.9.3. Qualitative observation using fluorescence microscopy and cardiac histopathology

Qualitative localization of Dox-CSEsNPs and DoxEs-CSEsNPs in different tissues was also observed in tumor bearing female rats. Dox presence was determined by their fluorescence emission from particular organ tissue using fluorescence microscopy (at 45×) after 6 h tail vein intravenous administration. As shown in Fig. 9, DoxEs-CSEsNPs formulation showed significant accumulation in the tumor tissue and insignificant accumulation in the heart and kidney compared with other formulation. These results might be attributed to the efficient interaction between estrone-conjugated Dox and cellular ERs [17] overexpressed on breast cancer cells [41]. The cardiac histopathology was also performed for the determination of Dox associated cardiac toxicity and is shown in Fig. 10. These images clearly showed that significant lower toxicity was shown by DoxEs, Dox-CSEsNPs and DoxEs-CSEsNPs formulation in comparison to free Dox. The study showed that it is

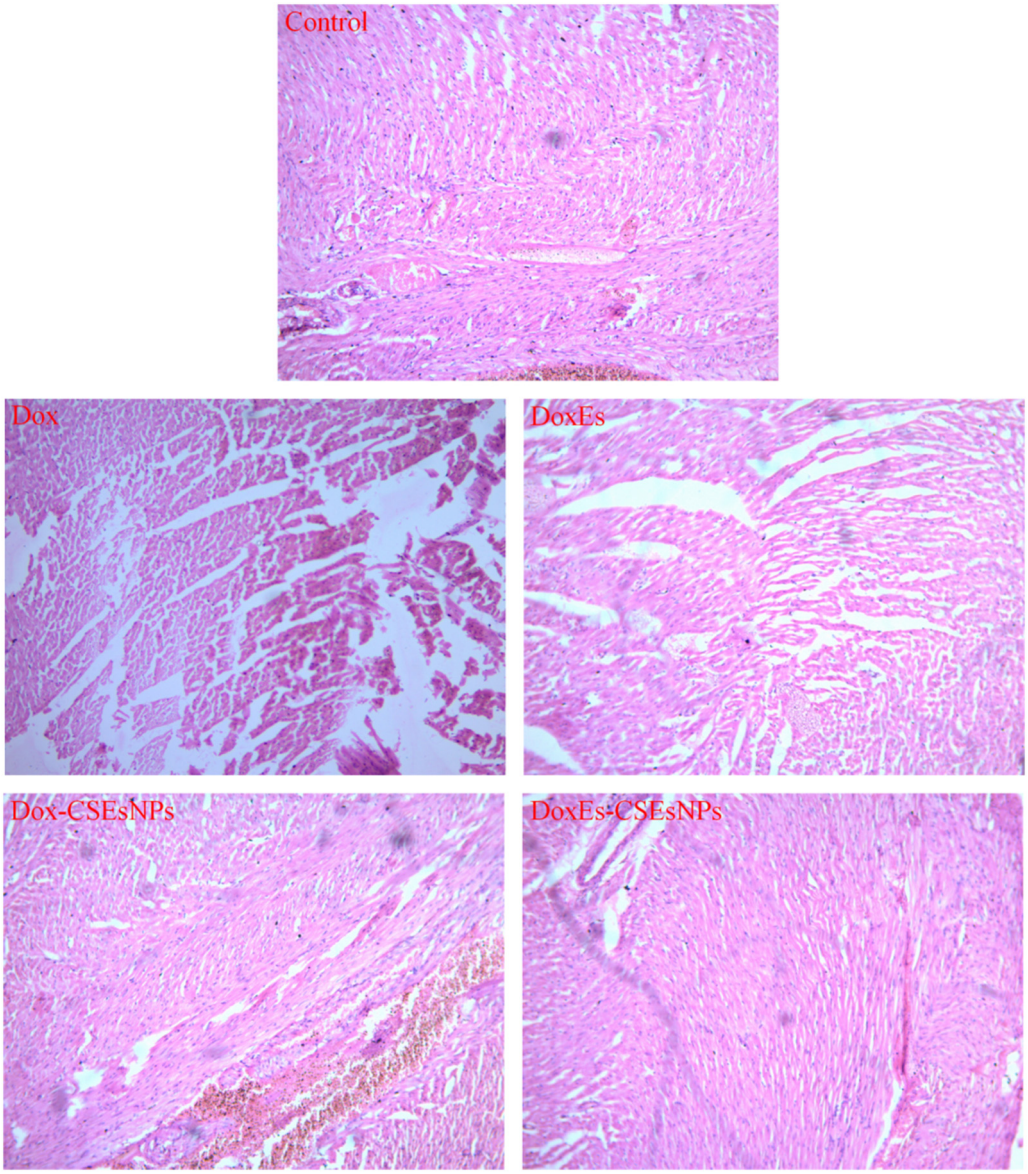

Fig. 10. Histopathological analysis image demonstrating cardiotoxicity of free Dox, DoxEs, Dox-CSEsNPs and DoxEs-CSEsNPs formulations (10×).

possible to achieve reduced cardiotoxicity due to Es conjugation and simultaneously encapsulation of Dox/Dox-Es in CSNPs [42]. Dual targeting could be useful in achieving the goal of magic bullet concept of targeted drug delivery for cancer therapy; more specifically breast cancer therapy using estrone as ligand for both intracellular and extracellular receptor in ER+ cancer.

4. Conclusion

The present work was aimed to develop targeted Dox delivery systems based on estrone chitosan conjugates nanoparticles. The use of targeting ligand (Es) for over-expressed tumor cell receptors is widely accepted as a concept and module, which may be used to selectively deliver therapeutic agents to these cells while sparing non-target healthy cells. Controlled and targeted Dox delivery with Es conjugation and uploading this conjugate in estrone chitosan conjugate-based nanoparticle can be a promising drug delivery strategy for anticancer bioactive to avoid the associated adverse effect as well as for potential therapeutic enhancement. Quality by Design approach has been successfully employed as unique tool for the optimization of nanoparticles formulations. It provides efficient understanding of the connection between in-process parameters to obtained better product quality i.e. PS, ZP, %EE and EE etc. The data obtained from in vitro studies and in vivo pharmacokinetic, and biodistribution studies also suggested that the Dox delivery with Es conjugation through estrone chitosan conjugates nanoparticles can be a promising drug delivery strategy for anticancer bioactive as a whole. The developed formulation could be useful in reducing the dosing frequency as well as dose. Further, it has been rendered least toxic against blood cells and cardiac tissues and this could help additionally in the reduction of cardiotoxicity of Dox. Hence, we propose that estrone-mediated biodisposition and cellular interaction of CSEsNPs, especially at the target sites would be useful and helpful for the upcoming research in the field of anticancer drug delivery.

CRediT authorship contribution statement

The role of contributing authors of this manuscript is as follows:
BDK: Data curation, Writing- Original draft preparation, Software.
RP: Software, Formal analysis, Writing- Reviewing and Editing.
SRP: Conceptualization, Methodology, Funding acquisition, Supervision, Investigation, Writing- Reviewing and Editing, Project administration.

List of abbreviations

BBD	Box–Behnken design
CS	Chitosan
DCC	Dicyclohexylcarbodiimide
DCM	Dichloromethane
DCU	N,N-dicyclohexylurea
DMAP	Dimethylaminopyridine
DMSO	Dimethyl sulfoxide
Dox	Doxorubicin
Dox-CSEsNPs	Dox containing estrone chitosan conjugates NPs
DoxEs	Dox and Es conjugate
DoxEs-CSEsNPs	DoxEs containing estrone chitosan conjugates NPs
DSC	Differential scanning calorimetry
EDC	N-(3-Dimethylaminopropyl)-N′-ethylcarbodiimide
ERs	Estrogen receptors
Es	Estrone
FT NMR	Fourier-Transform NMR
FTIR	Fourier-transform infrared spectroscopy
H	Hour
HPLC	High-performance liquid chromatography
IR	Infrared
MCF-7	Michigan Cancer Foundation-7
mL	Milliliter
mmol	Millimoles
MWCO	Molecular weight cut-off
NaOH	Sodium hydroxide
NH_2	Amino
NHS	N hydroxysuccinimide
NMR	Nuclear magnetic resonance
NPs	Nanoparticles
PDI	Polydispersity index
PS	Particle size
QbD	Quality by Design
RGD	Arginine-Glycine-Aspartic acid
SA	Succinic anhydride
SM	Surface morphology
TEA	Triethylamine
TPP	Sodium tripolyphosphate
TRs	Transferrin receptors
ZP	Zeta-potential

Declaration of competing interest

The authors confirm that this article content has no conflict of interest.

Acknowledgement

This work is supported by Science and Engineering Research Board, Department of Science and Technology, India (SB/YS/LS-333/2013) to SRP in the form of young scientist project grant. BDK is thankful for providing research fellowship to the agency.

Appendix A. Supplementary data

Supplementary data to this article can be found online at https://doi.org/10.1016/j.ijbiomac.2020.08.172.

References

[1] R.L. Siegel, K.D. Miller, A. Jemal, Cancer statistics, 2017, CA Cancer J. Clin. 67 (1) (2017) 7–30, https://doi.org/10.3322/caac.21387.
[2] P. Tekchandani, B.D. Kurmi, S.R. Paliwal, Nanomedicine to deal with cancer cell biology in multi-drug resistance, Mini-Rev. Med. Chem. 17 (18) (2017) 1793–1810, https://doi.org/10.2174/1389557516666160219123222.
[3] R. Munagala, F. Aqil, R.C. Gupta, Promising molecular targeted therapies in breast cancer, Indian J. Pharm. 43 (3) (2011) 236–245, https://doi.org/10.4103/0253-7613.81497.
[4] B.D. Kurmi, P. Patel, R. Paliwal, S.R. Paliwal, Technology, molecular approaches for targeted drug delivery towards cancer: a concise review with respect to nanotechnology, J. Drug Deliv. Sci. Technol. (2020) 101682, https://doi.org/10.1016/j.jddst.2020.101682.
[5] V. Masoud, G. Pages, Targeted therapies in breast cancer: new challenges to fight against resistance, World J. Clin. Oncol. 8 (2) (2017) 120–134, https://doi.org/10.5306/wjco.v8.i2.120.
[6] D.C. Marquez, R.J. Pietras, Membrane-associated binding sites for estrogen contribute to growth regulation of human breast cancer cells, Oncogene 20 (39) (2001) 5420–5430, https://doi.org/10.1038/sj.onc.1204729.
[7] F.A. Holmes, R.S. Walters, R.L. Theriault, A.D. Forman, L.K. Newton, M.N. Raber, et al., Phase II trial of taxol, an active drug in the treatment of metastatic breast cancer, J. Natl. Cancer Inst. 83 (24) (1991) 1797–1805, https://doi.org/10.1093/jnci/83.24.1797-a.
[8] R.W. Boyle, C.K. Johnson, D. Dolphin, Iodination and heck alkynylation of 5,15-diphenylporphyrin. A convenient entry to asymmetrically meso-substituted porphyrins, J. Chem. Soc. Chem. Commun. (5) (1995) 527–528, https://doi.org/10.1039/C39950000527.
[9] S.R. Paliwal, R. Paliwal, N. Mishra, A. Mehta, S.P. Vyas, A novel cancer targeting approach based on estrone anchored stealth liposome for site-specific breast cancer therapy, Curr. Cancer Drug Targets 10 (3) (2010) 343–353, https://doi.org/10.2174/156800910791190210.
[10] S.R. Paliwal, R. Paliwal, H.C. Pal, A.K. Saxena, P.R. Sharma, P.N. Gupta, et al., Estrogen-anchored pH-sensitive liposomes as nanomodule designed for site-specific delivery of doxorubicin in breast cancer therapy, Mol. Pharm. 9 (1) (2012) 176–186, https://doi.org/10.1021/mp200439z.
[11] B.S. Reddy, R. Banerjee, 17Beta-estradiol-associated stealth-liposomal delivery of anticancer gene to breast cancer cells, Angew. Chem. Int. Ed. Eng. 44 (41) (2005) 6723–6727, https://doi.org/10.1002/anie.200501793.
[12] B.D. Kurmi, J. Kayat, V. Gajbhiye, R.K. Tekade, N.K. Jain, Micro- and nanocarrier-mediated lung targeting, Expert Opin. Drug Deliv. 7 (7) (2010) 781–794, https://doi.org/10.1517/17425247.2010.492212.
[13] F.Y. Samadi, Z. Mohammadi, M. Yousefi, S. Majdejabbari, Synthesis of raloxifene-chitosan conjugate: a novel chitosan derivative as a potential targeting vehicle, Int. J. Biol. Macromol. 82 (2016) 599–606, https://doi.org/10.1016/j.ijbiomac.2015.10.041.
[14] J. Prados, C. Melguizo, R. Ortiz, C. Velez, P.J. Alvarez, J.L. Arias, et al., Doxorubicin-loaded nanoparticles: new advances in breast cancer therapy, Anti Cancer Agents Med. Chem. 12 (9) (2012) 1058–1070, https://doi.org/10.2174/187152012803529646.
[15] S. Rai, R. Paliwal, B. Vaidya, P.N. Gupta, S. Mahor, K. Khatri, et al., Estrogen(s) and analogs as a non-immunogenic endogenous ligand in targeted drug/DNA delivery, Curr. Med. Chem. 14 (19) (2007) 2095–2109, https://doi.org/10.2174/092986707781368432.
[16] A. Kaur, B.S. Bhoop, S. Chhibber, G. Sharma, V.S. Gondil, O.P. Katare, Supramolecular nano-engineered lipidic carriers based on diflunisal-phospholipid complex for transdermal delivery: QbD based optimization, characterization and preclinical investigations for management of rheumatoid arthritis, Int. J. Pharm. 533 (1) (2017) 206–224, https://doi.org/10.1016/j.ijpharm.2017.09.041.
[17] S. Rai, R. Paliwal, B. Vaidya, K. Khatri, A.K. Goyal, P.N. Gupta, et al., Targeted delivery of doxorubicin via estrone-appended liposomes, J. Drug Target. 16 (6) (2008) 455–463, https://doi.org/10.1080/10611860802088481.
[18] N. Cao, S.S. Feng, Doxorubicin conjugated to D-alpha-tocopheryl polyethylene glycol 1000 succinate (TPGS): conjugation chemistry, characterization, in vitro and in vivo evaluation, Biomaterials 29 (28) (2008) 3856–3865, https://doi.org/10.1016/j.biomaterials.2008.05.016.
[19] Y. Guo, M. Chu, S. Tan, S. Zhao, H. Liu, B.O. Otieno, et al., Chitosan-g-TPGS nanoparticles for anticancer drug delivery and overcoming multidrug resistance, Mol. Pharm. 11 (1) (2014) 59–70, https://doi.org/10.1021/mp400514t.
[20] S. Wadhwa, R. Paliwal, S.R. Paliwal, S.P. Vyas, Hyaluronic acid modified chitosan nanoparticles for effective management of glaucoma: development, characterization, and evaluation, J. Drug Target. 18 (4) (2010) 292–302, https://doi.org/10.3109/10611860903450023.
[21] B.D. Kurmi, V. Gajbhiye, J. Kayat, N.K. Jain, Lactoferrin-conjugated dendritic nanoconstructs for lung targeting of methotrexate, J. Pharm. Sci. 100 (6) (2011) 2311–2320, https://doi.org/10.1002/jps.22469.
[22] L.M. Rose, K.F. Tillery, S.M. el Dareer, D.L. Hill, High-performance liquid chromatographic determination of doxorubicin and its metabolites in plasma and tissue, J. Chromatogr. 425 (2) (1988) 419–423, https://doi.org/10.1016/0378-4347(88)80049-5.
[23] M. Habib-ur-Rehman, M. Tahir, K.P. Lone, W. Sami, Ethanol induced hepatotoxicity in albino rats, J. Coll. Physicians Surg. Pak. 21 (10) (2011) 642–643, https://doi.org/10.2011/JCPSP.642643.
[24] D. Mishra, N. Jain, V. Rajoriya, A.K. Jain, Glycyrrhizin conjugated chitosan nanoparticles for hepatocyte-targeted delivery of lamivudine, J. Pharm. Pharmacol. 66 (8) (2014) 1082–1093, https://doi.org/10.1111/jphp.12235.
[25] R. Gao, X. Su, X. He, L. Chen, Y. Zhang, Preparation and characterisation of core-shell CNTs@MIPs nanocomposites and selective removal of estrone from water samples, Talanta 83 (3) (2011) 757–764, https://doi.org/10.1016/j.talanta.2010.10.034.

[26] R. Paliwal, S.R. Paliwal, K. Sulakhiya, B.D. Kurmi, R. Kenwat, A. Mamgain, Chitosan-based nanocarriers for ophthalmic applications, in: S. Maiti, S. Jana (Eds.), Polysaccharide Carriers for Drug Delivery, Elsevier 2019, pp. 79–104.
[27] A. Czyrski, J. Sznura, The application of Box-Behnken-design in the optimization of HPLC separation of fluoroquinolones, Sci. Rep. 9 (1) (2019), 19458https://doi.org/10.1038/s41598-019-55761-z.
[28] S.-N. Nam, H. Cho, J. Han, N. Her, J. Yoon, Photocatalytic degradation of acesulfame K: optimization using the Box–Behnken design (BBD), Process. Saf. Environ. Prot. 113 (2018) 10–21, https://doi.org/10.1016/j.psep.2017.09.002.
[29] F. Haghiralsadat, G. Amoabediny, M.H. Sheikhha, B. Zandieh-Doulabi, S. Naderinezhad, M.N. Helder, et al., New liposomal doxorubicin nanoformulation for osteosarcoma: drug release kinetic study based on thermo and pH sensitivity, Chem. Biol. Drug Des. 90 (3) (2017) 368–379, https://doi.org/10.1111/cbdd.12953.
[30] D.M. Benival, P.V. Devarajan, Lipomer of doxorubicin hydrochloride for enhanced oral bioavailability, Int. J. Pharm. 423 (2) (2012) 554–561, https://doi.org/10.1016/j.ijpharm.2011.11.035.
[31] S. Tummala, M.N. Satish Kumar, A. Prakash, Formulation and characterization of 5-fluorouracil enteric coated nanoparticles for sustained and localized release in treating colorectal cancer, Saudi Pharm. J. 23 (3) (2015) 308–314, https://doi.org/10.1016/j.jsps.2014.11.010.
[32] R. Paliwal, S.R. Paliwal, G.P. Agrawal, S.P. Vyas, Chitosan nanoconstructs for improved oral delivery of low molecular weight heparin: in vitro and in vivo evaluation, Int. J. Pharm. 422 (1–2) (2012) 179–184, https://doi.org/10.1016/j.ijpharm.2011.10.048.
[33] L. Zhao, G. Yang, Y. Shi, C. Su, J. Chang, Co-delivery of Gefitinib and chloroquine by chitosan nanoparticles for overcoming the drug acquired resistance, J. Nanobiotechnol. 13 (2015) 57, https://doi.org/10.1186/s12951-015-0121-5.
[34] V. Kamat, I. Marathe, V. Ghormade, D. Bodas, K. Paknikar, Synthesis of monodisperse chitosan nanoparticles and in situ drug loading using active microreactor, ACS Appl. Mater. Interfaces 7 (41) (2015) 22839–22847, https://doi.org/10.1021/acsami.5b05100.
[35] R.L. Ding, F. Xie, Y. Hu, S.Z. Fu, J.B. Wu, J. Fan, et al., Preparation of endostatin-loaded chitosan nanoparticles and evaluation of the antitumor effect of such nanoparticles on the Lewis lung cancer model, Drug Deliv. 24 (1) (2017) 300–308, https://doi.org/10.1080/10717544.2016.1247927.
[36] R. Rukmangathen, I.M. Yallamalli, P.R. Yalavarthi, Biopharmaceutical potential of selegiline loaded chitosan nanoparticles in the management of Parkinson's disease, Curr. Drug Discov. Technol. 16 (4) (2019) 417–425, https://doi.org/10.2174/1570163815666180418144019.
[37] K. Rajpoot, S.K. Jain, Colorectal cancer-targeted delivery of oxaliplatin via folic acid-grafted solid lipid nanoparticles: preparation, optimization, and in vitro evaluation, Artif. Cells Nanomed. Biotechnol. 46 (6) (2018) 1236–1247, https://doi.org/10.1080/21691401.2017.1366338.
[38] K. Jain, N.K. Jain, Surface engineered dendrimers as antiangiogenic agent and carrier for anticancer drug: dual attack on cancer, J. Nanosci. Nanotechnol. 14 (7) (2014) 5075–5087, https://doi.org/10.1166/jnn.2014.8677.
[39] D. Guo, C. Shi, X. Wang, L. Wang, S. Zhang, J. Luo, Riboflavin-containing telodendrimer nanocarriers for efficient doxorubicin delivery: high loading capacity, increased stability, and improved anticancer efficacy, Biomaterials 141 (2017) 161–175, https://doi.org/10.1016/j.biomaterials.2017.06.041.
[40] C.S. Porto, G.L. Gunsalus, C.W. Bardin, D.M. Phillips, N.A. Musto, Receptor-mediated endocytosis of an extracellular steroid-binding protein (TeBG) in MCF-7 human breast cancer cells, Endocrinology 129 (1) (1991) 436–445, https://doi.org/10.1210/endo-129-1-436.
[41] S.A. Fuqua, Y. Cui, Targeting the estrogen receptor in clinical breast cancer, Breast Dis. 15 (2002) 3–11, https://doi.org/10.3233/bd-2002-15102.
[42] L. Polgar, E. Lajko, P. Soos, O. Lang, M. Manea, B. Merkely, et al., Drug targeting to decrease cardiotoxicity - determination of the cytotoxic effect of GnRH-based conjugates containing doxorubicin, daunorubicin and methotrexate on human cardiomyocytes and endothelial cells, Beilstein J. Org. Chem. 14 (2018) 1583–1594, https://doi.org/10.3762/bjoc.14.136.